Technical Report

Nr.: FIN-006-2009

Automatic Transfer Function Specification for Visual Emphasis of Coronary Artery Plaque

S. Glaßer, S. Oeltze, A. Hennemuth, C. Kubisch, A. Mahnken, S. Wilhelmsen, B. Preim

Arbeitsgruppe Visualisierung

Fakultät für Informatik
Otto-von-Guericke-Universität Magdeburg

Nr.: FIN-006-2009

Automatic Transfer Function Specification for Visual Emphasis of Coronary Artery Plaque

S. Glaßer, S. Oeltze, A. Hennemuth, C. Kubisch, A. Mahnken,
S. Wilhelmsen, B. Preim

Arbeitsgruppe Visualisierung

Fakultät für Informatik
Otto-von-Guericke-Universität Magdeburg

Impressum (§ 5 TMG):

Herausgeber:
Otto-von-Guericke-Universität Magdeburg
Fakultät für Informatik
Der Dekan

Verantwortlich für diese Ausgabe:
Otto-von-Guericke-Universität Magdeburg
Fakultät für Informatik
Sylvia Glaßer
Postfach 4120
39016 Magdeburg
E-Mail: glasser@isg.cs.uni-magdeburg.de

http://www.cs.uni-magdeburg.de/Preprints.html

Auflage: 61

Redaktionsschluss: 08.04.2009

Herstellung: Dezernat Allgemeine Angelegenheiten,
Sachgebiet Reproduktion

Bezug: Universitätsbibliothek/Hochschulschriften- und
Tauschstelle

Automatic Transfer Function Specification for Visual Emphasis of Coronary Artery Plaque

S. Glaßer[1], S. Oeltze[1], A. Hennemuth[2], C. Kubisch[1], A. Mahnken[3], S. Wilhelmsen[4], and B. Preim[1]

[1]Department of Simulation and Graphics, University of Magdeburg
[2]MeVis Research GmbH, Bremen
[3]Department of Radiology, University Hospital, Magdeburg
[4]Department of Radiology, University Hospital, Aachen University of Technology

Abstract

Cardiovascular imaging with current multislice spiral computed tomography (MSCT) technology enables a non-invasive evaluation of the coronary arteries. Contrast-enhanced MSCT angiography with high spatial resolution allows for a segmentation of the coronary artery tree. We present an automatically adapted transfer function (TF) specification to highlight pathologic changes of the vessel wall based on the segmentation result of the coronary artery tree. The TFs are combined with common visualization techniques, such as multiplanar reformation and direct volume rendering for the evaluation of coronary arteries in MSCT image data. The presented TF-based mapping of CT values in Hounsfield Units (HU) to color and opacity leads to a different color coding for different plaque types. To account for varying HU values of the vessel lumen caused by the contrast medium, the TFs are adapted to each dataset by local histogram analysis. We describe an informal evaluation with three board-certified radiologists which indicates that the represented visualizations guide the user's attention to pathologic changes of the vessel wall as well as provide an overview about spatial variations.

1. Introduction

Coronary artery disease (CAD) is the leading cause of death in western nations [Ame07]. For CAD diagnosis, several image modalities are applied, e.g. conventional x-ray angiography, magnetic resonance imaging and computed tomography (CT) of the heart. Recent developments in multislice spiral computed tomography (MSCT) allow for a high spatial resolution with short acquisition times [SB*04]. Contrast-enhanced CT coronary angiography (CTA) allows to reliably exclude CAD. Especially for asymptomatic patients, who have a high CAD risk (due to increased blood pressure, age, gender and stress), CTA is the image modality of choice. CTA image data also enable an assessment of the vessel's cross-sectional area and have a great potential for noninvasive identification, characterization, and quantification of atherosclerotic CAD [SB*04]. Atherosclerotic CAD is the result of accumulations in the coronary artery wall, so-called plaques.

Plaque deposits are small structures with inhomogeneous densities inside the vessel wall and cannot be segmented directly in CTA datasets. Therefore, we aim for a visual emphasis of coronary artery plaques in CTA datasets using a transfer function (TF). To account for varying CT values of the bloodpool due to the non-uniform spatial diffusion of the contrast medium, the TF has to be adapted to each dataset. We perform this adaption automatically based on a coarse segmentation of the coronary artery tree. We carry out a local histogram analysis for the segmentation result and further employ a local histogram analysis of the vessel wall based on the coronary arteries' centerline as well. This enables us to visualize the coronary vessel wall containing coronary artery plaque. Furthermore, the TFs are combined with common visualization techniques for CTA datasets. Common techniques for the visualization of the coronary artery tree based on CTA image data are maximum intensity projection (MIP), multiplanar reformation (MPR), curved multiplanar reconstruction (CPR) [KFW*02] for 2D views and direct volume rendering techniques (DVR) for a 3D view.

2. Medical Background

Atherosclerotic plaques can be classified into soft, fibrous and hard plaques. Soft plaques are prone to rupture and thus very dangerous for the patient, whereas fibrous plaques and hard plaques consist of more dense accumulations and are more stable. In addition, hard plaque deposits contain calcium accumulations. Non-enhanced MSCT is primarily used for the detection of the coronary arterial calcium. The overall coronary calcium acts as an indicator for the patient's whole plaque burden and can be quantified, e.g. with the Agatston calcium score [AJH*90].

CTA datasets better depict the blood and allow for a differentiation of calcified and noncalcified plaques and for an assessment of stenoses. A stenosis is a narrowing of the lumen – the vessel's inner open area. CTA has been established for patients with abnormal coronary spatial variation. Furthermore, it is employed for monitoring coronary stents and coronary bypasses. The early stages of atherosclerotic CAD do not necessarily lead to significant stenoses, see Fig. 1. Therefore, the evaluation of the coronary artery lumen is insufficient for the assessment of the patient's plaque burden and the pathologic change of the vessel wall has to be taken into account. Oblique MPRs enable a cross-sectional view of the coronary artery and its wall along the vessel's centerline, whereas CPRs provide the vessel's longitudinal view [KFW*02].

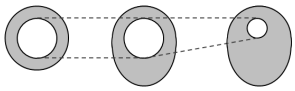

Figure 1: *Illustration of remodeling in vessel cross-section. Normal vessel with normal vessel wall (grey) is depicted (left). Early stages of CAD are compensated by positive remodeling – the increasing vessel wall thickness (middle). The negative remodeling, caused by progressive CAD, leads to a stenosis (right).*

DVR techniques convey information on the complex anatomy of the entire coronary tree. However, these visualizations provide only limited information about pathologic vessel wall changes and the coronary artery lumen. Modern workstations employ predefined TFs for the visualization of the heart and the coronary arteries in CTA datasets. Our approach aims at a more sophisticated DVR parameterization to provide a fast overview of existing stents and calcified plaques and thus indicate the patient's whole plaque burden.

3. Related Work

There is a large variety of techniques for visualizing vasculature which can be grouped into surface rendering (SR) and DVR approaches. SR relies on the extraction of vascular structures, e.g. by thresholding or explicit segmentation, and converts the result to a polygonal mesh (see [PO07] for an overview). For the evaluation of CAD, we consider that SR is not appropriate since small inhomogeneous plaque deposits inside the vessel wall as well as the vessel wall itself could not be reliably extracted. Therefore, SR would lead to an accuracy in the visualization, which does not correspond to the underlying data. Furthermore, transitions in the TF domain may not be represented with SR. We therefore use DVR techniques as has been suggested in [vOvGR*03].

Vega et al. [VST*03, VST*04] discuss the automatic design of 2D TFs to emphasize vascular structures based on intensity values and gradient magnitude. Their approach allows to discriminate bones and vascular structures in the brain. However, it is not able to emphasize abnormalities at the vessel wall. Our concept is similar to [LLY05], who use local histogram analysis to differentiate between organ tissues.

With DVR, surfaces of interest are indirectly classified using TFs. There exist special approaches to support the interactive definition of TFs for specialized viualizations [KKH02]. To avoid the considerable interobserver variability, we aim at an automatically defined TF as starting point for further exploration. In addition to image data values, derived information such as gradient magnitude [KKH02] or distance to some reference structure [TPD06] can be employed resulting in multidimensional TFs. Tests revealed that gradient magnitude can help to enhance the boundary between bloodpool and surrounding tissue. The highlighting of the vessel wall itself could not be improved due to its small extent and thus high sensitivity to noise and the partial volume effect. Distance-based TFs are also inappropriate since the remodeling of the vessel wall leads to varying lumen diameters resulting in varying distances to the vessel centerline. Another approach was presented by [CM08], who employed scale fields for the generation of size-based TFs.

Visualization of internal structures with simple TFs has been performed by [RSK06] using a layering technique. However, this approach was not considered applicable as the authors have stated that accuracy was less important than interactivity. For CAD diagnosis, accuracy is critical. Hence, more intensive preprocessing such as segmentation and TF computation are justified. For the visualization of coronary arteries in CTA data, the combination of different views supports the evaluation of the vessels, as shown in [KHB*06] and [SCC*04]. In both approaches, DVR views are used for providing spatial information, whereas the vessels can be evaluated in more detail in the 2D CPR or MPR views.

MIP views of contrast-enhanced vessels in medical image data, e.g. the MIP views of segmented objects [BA02] or sliding-thin-slab-MIPs [NRJ93] could also be considered as imaging method for CAD evaluation. We do not use MIP visualizations, since we focus on the vessel wall and not the lumen. Visual separation of hard plaques in CTA datasets

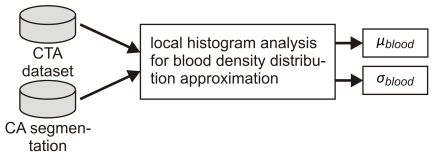

Figure 2: *Automatic approximation of the parameters μ_{blood} and σ_{blood}. The parameters are calculated by analyzing the local histogram of the coronary artery (CA) segmentation result.*

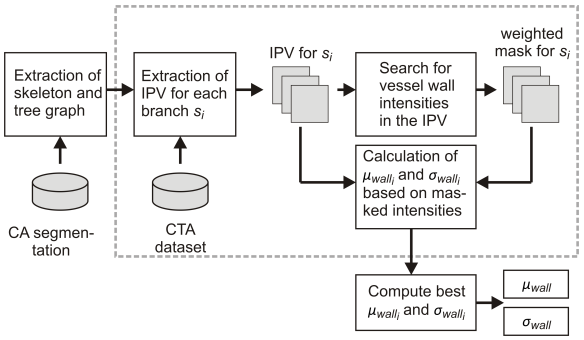

Figure 3: *Automatic approximation of the parameters μ_{wall} and σ_{wall}. The parameters are chosen from the set of μ_{wall_i} and σ_{wall_i} for all branches b_i. First, the centerline of the CA segmentation is extracted. The centerline is used to identify branches of the CA tree. Second, for each branch b_i an intensity profile volume (IPV) is extracted. Based on the IPV a weighted mask for masking all vessel wall intensities is determined. The weighted mask is applied to the IPV and yields a sample set of vessel wall intensities which is used for calculating μ_{wall_i} and σ_{wall_i} for b_i.*

supports the fast evaluation of the patient's plaque burden. Hong et al. [HBS*02] applied calcium scores to CTA image datasets, yielding a threshold of 350 HU for hard plaqe separation. Wesarg et al. [WFKF06] detected hard plaques in CTA datasets by analysing the minimal diameter of the vessel lumen and examining stenotic regions. The separation of the stenotic hard plaque deposits depends on the mean intensity of a voxel representing the contrast-enhanced lumen. Furthermore, Wesarg et al. presented a visualization with a highlighting of stenoses by simultaneously mapping the minimal lumen diameter to color and to the diameter of a tube around the vessel. The automatic detection and separation of soft and fibrous plaques is difficult, since clinical studies provide different and sometimes overlapping HU intervals for these plaque types [PAM*07].

4. Concept

We present an automatic TF specification for visual emphasis of soft and fibrous plaques and for a visual separation of hard plaques and coronary stents. In contrast to conventional methods, we highlight the vessel wall instead of the contrast-enhanced lumen of the coronary arteries, including stenotic and non-stenotic plaques. Our TF specification is based on the segmented coronary arteries, extracted with the method described in [HBF*05], of a CTA dataset. The TF specification is carried out by determining supporting points, which depend on the mean intensity and standard deviation of the bloodpool (μ_{blood}, σ_{blood}) and the vessel wall (μ_{wall}, σ_{wall}). These parameters are fully automatically approximated (see Fig. 2). The blood intensity distribution is calculated by analyzing the local histogram of the coronary artery segmentation result. For the vessel wall intensity distribution, a further local histogram analysis is employed (see Fig. 3). The local histogram of vessel wall intensities is based on the centerline of the segmentation result. For each branch, an intensity profile volume (IPV) and a weighted mask, masking all vessel wall intensities, is extracted. The weighted mask is applied to the IPV and yields the local histogram of the vessel wall intensities, which is used for the calculation of μ_{wall} and σ_{wall}. The different steps are described in the following.

4.1. Approximation of the Blood Intensity Distribution

The segmentation result mainly consists of voxels representing the contrast-enhanced blood and is used for the approximation of the blood intensity distribution. The parameters μ_{blood} and σ_{blood} cannot directly be derived from the sample containing all segmented voxels, because of other intensities originating from surrounding tissue or interpolation issues.

The approximation is carried out by means of an iterative fitting of a normal distribution to the distribution of all segmented voxels. We defined a cost function as the sum of differences for each HU value. We employ binary search methods to find the parameters which lead to the smallest costs. Results for μ_{blood} and σ_{blood} indicate that the mean intensity of the blood strongly differs for each dataset (i.e. $\mu_{blood} \in [218HU, 478HU]$ for all tested datasets). Thus, a static threshold for hard plaque separation from contrast-enhanced blood for all datasets is not applicable. We use a dynamic threshold similar to the Agatston score [AJH*90]. The Agatston score defines the threshold for hard plaques as the sum of the mean plus twice the standard deviation of the non-enhanced blood intensity. We experienced an overestimation using this threshold, which may arise due to artifacts or contrast medium accumulations in small branches. We therefore empirically determined the threshold $\mu_{blood} + 3\sigma_{blood}$ using the knowledge of hard plaque localizations. Coronary stents, which have similar x-ray attenuation coefficients as hard plaques, will be highlighted in the same manner.

4.2. Approximation of the Vessel Wall Intensity

The described method for approximating the blood intensity is not applicable for the vessel wall, since the voxels representing the vessel wall cannot be separated in a histogram of the segmentation result. For the vessel wall intensity approximation, we employ a local histogram analysis for each coronary artery branch (see Fig. 3). To identify these branches, the centerline of the segmented coronary arteries is generated. We employ a successive erosion of border voxels, also taking anisotropic voxel extents into account, whereas the topology of the initial mask is preserved, as presented by Selle [SPSP02]. The centerline is transformed into a primitive tree graph representation, whereas each branch consists of a list with the corresponding voxels and a list to the next branches.

For each branch and its corresponding centerline, a local histogram is generated via IPV extraction. For each voxel centerline, n rays perpendicular to it are casted and sampled in the CTA dataset. The number of rays (n) can be manipulated, depending on the voxel size and the diameter of coronary arteries, which tapers down from $5mm$ to $1mm$. We empirically determine an amount of 16 rays for each tested dataset (with voxel size of $\approx 0.3mm \times 0.3mm \times 0.4mm$) and a stepsize of half of the smallest voxel extent. The rays are sampled with the stepsize for a certain distance, e.g. $3mm$, whereas $2.5mm$ is the maximum radius of coronary arteries. The sampled intensities are stored in a slice of the IPV (see Fig. 4). By repeating this procedure for all centerline voxels, an IPV with a slice number that equals the number of centerline voxels is created.

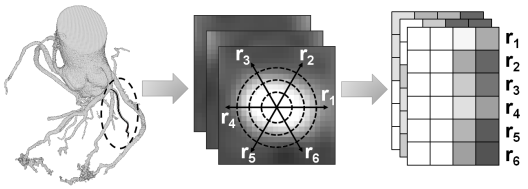

Figure 4: *Extraction of the IPV. For each voxel of the centerline of a coronary branch (left), n (e.g. 6) rays perpendicular to the centerline are casted (middle). Along the rays, intensities are sampled and stored in a slice of the IPV (right). Repeating this procedure for each centerline voxel of the branch yields the IPV.*

For the determination of the vessel wall intensities, we employ a slicewise search for vertical structures to the IPV. Since sampled intensities, which exhibit the same distances to the centerline voxel will appear as verticals in the IPV slice for this voxel, intensities representing the vessel wall will also be arranged in a vertical order. These vertical edges can be heavily distorted due to the approximation of the centerline of the branch by the centerline of the segmentation, coronary artery wall remodeling, as well as artifacts arising from dense structures such as hard plaques (see Fig. 5).

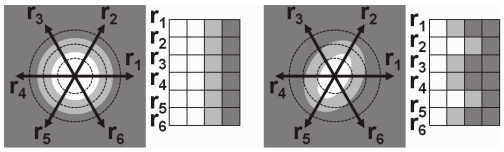

Figure 5: *Schemes of cross-sectional vessel views. The casting of rays with the origin at the centerline in contrast-enhanced lumen (white) across the vessel wall (light grey) to surrounding tissue (dark grey) is illustrated. Ideally, circle-like cross-sections yield a vertical in the corresponding IPV slice (left), whereas ellipsoidal cross-sections lead to distorted vertical structures (right).*

Vertical structures can be enhanced by a slicewise convolution of the IPV with a Laplacian of Gaussian (LoG) filter. Due to its small size, the partial volume effect has a strong influence on the vessel wall. Therefore, the LoG filter with kernelsize 3×3 first smoothes the data of the IPV slice and then approximates the gradient magnitude. In the next step, a slicewise normalization and thresholding removes intensities with small gradient magnitudes. We use a threshold of 0.5 for the normalized slices, which yields a binary mask that marks all intensities with a higher gradient magnitude. For taking also distorted vertical structures into account, we apply a weight function f_w to the voxels of each binary mask slice. It is defined as:

$$f_W = \begin{cases} 0 & if \quad \frac{\sum column}{n} < 0.5 \\ \frac{\sum column}{n} & else \end{cases} \tag{1}$$

where n is the length of each column, i.e. the number of rays that were casted, and $\sum column$ is the number of fields, which are marked by the binary mask in this column. The sample set of the vessel wall intensities is determined by employing the f_W weighted binary mask to the original IPV yielding intensities d_i with weights w_i, where w_i is the sum of all weights assigned by f_W for the density d_i.

For each branch b_i of the coronary artery tree we determine μ_{wall_i} and σ_{wall_i}. We then consider the branch b_i with the longest centerline and whose parameters μ_{wall_i} and σ_{wall_i} fulfill the condition $\mu_{wall_i} < \mu_{blood} - 2\sigma_{blood}$, as best candidate for defining a global TF. For the tested datasets, μ_{wall} was in the intervall $[50HU, 270HU]$. The parameter extraction took in average ≈ 4 min for each dataset and was carried out on a 3.06GHz processor with 3GB of RAM.

4.3. TF Specification

The TF specification is based on supporting points, which depend on the parameters μ_{wall}, σ_{wall}, μ_{blood} and σ_{blood}. For each point, we define an opacity and a color value. Between

these supporting points, opacity and colors are linearly interpolated. Basically, all TFs which highlight the vessel wall intensities and provide a visual separation of hard plaques (i.e. intensities $> \mu_{blood} + 3\sigma_{blood}$ as described in subsection 4.1) will be considered as sufficient. Furthermore, transparency should be assigned to the vessel wall's intensities to reveal inner structures. Full transparency can be assigned to the surrounding tissue and the contrast-enhanced blood.

Color assignment to the supporting points aims at visual separation of hard plaques and stents and high contrasts for the vessel wall visualization. Since hard plaques and stents are very dense structures, they usually appear white or light grey in conventional CTA views. The visual separation is achieved by employing colors from beige to white in combination with high opacity values. For the vessel wall, a color scale from blue over red to green should be applied, yielding high contrasts for the visualization of different vessel wall intensities and thus different plaque deposits. Furthermore, low contrast between the vessel's outer boundary and surrounding tissue is necessary, since a reliable segmentation of the whole coronary artery vessel wall is absent. A high contrast discontinuity in the TF would imply too much accuracy on the exact location of the wall.

We define two TFs depending on the dimensionality of the viewer: the TF_{2D} and the TF_{3D}. To avoid occlusions in the 3D case, we use the interval size $\mu_{wall} \pm \sigma_{wall}$ for the TF_{3D} and $\mu_{wall} \pm 2\sigma_{wall}$ for the TF_{2D}. We present one (of potentially several) solutions to our requirements by defining nine sample points $S_0 - S_8$ (see Tab. 1 and Fig. 6).

TF_{3D}	
S_0	$-1024HU$
S_1	$S_3 - \sigma_{wall}$
S_2	$S_3 - \frac{1}{4}\sigma_{wall}$
S_3	μ_{wall}
S_4	$S_3 + \frac{1}{4}\sigma_{wall}$
S_5	$\mu_{blood} - 2\sigma_{blood}$
S_6	$\mu_{blood} + 3\sigma_{blood}$
S_7	$S_6 + \sigma_{blood}$
S_8	$3071HU$

TF_{2D}	
S_0	$-1024HU$
S_1	$S_3 - 2\sigma_{wall}$
S_2	$S_3 - \sigma_{wall}$
S_3	μ_{wall}
S_4	$\frac{1}{2}(S_3 + S_5)$
S_5	$\mu_{blood} - 2\sigma_{blood}$
S_6	$\mu_{blood} + 3\sigma_{blood}$
S_7	$S_6 + \sigma_{blood}$
S_8	$3071HU$

Table 1: *Supporting point calculation for TF_{3D} and TF_{2D}. S_6 is the supporting point for hard plaque separation, as described in subsection 4.1.*

While in DVR visualization the TF_{3D} is solely applied, in the 2D CPR and MPR views the TF_{2D} can be combined with a standard greyscale visualization. As no occlusion occurs in the 2D views, the TF_{2D} is overlaid by a conventional slice view to highlight the vessel wall and to provide contextual information of the unmasked data. The lookup table of the windowing TF is therefore blended, i.e. linearly interpolated, with the lookup table of the TF_{2D}, whereas the opacity value determines the influence of the TF_{2D} (see Fig. 7). The user can manipulate the windowing TF's parameters and thus directly influence brightness and contrast of the combined TF_{2D}.

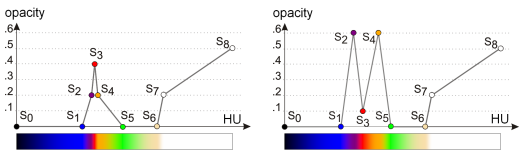

Figure 6: *Graphs of the TF_{3D} (left) and TF_{2D} (right). Specification is carried out by calculation of μ_{wall}, σ_{wall}, μ_{blood} and σ_{blood} and thus the supporting points S_0 - S_8. Opacity values are linearly interpolated between the points. The HU values differ from dataset to dataset. Therefore, the x-axis is not labeled.*

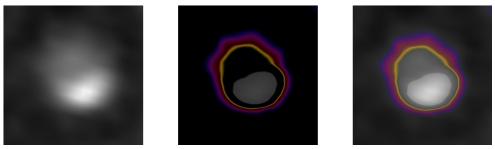

Figure 7: *Combination of the windowing TF and the TF_{2D} by blending. On the left, the MPR view with a hard plaque (white area) is visualized by employing a ramp. In the middle, the TF_{2D} was applied an on the right, the combination of TF_{2D} and windowing TF was used.*

To enhance the dataset exploration, the user can slightly change the automatically adapted TFs. Therefore, an offset for S_6 and S_3 can be manipulated, with the other supporting points being updated accordingly. The user can manipulate the visual separation of hard plaques as well as the region of highlighted vessel wall intensities, which may be necessary to cope with artifacts in selected datasets and allows for quality judgement.

4.4. Rendering of the 3D DVR View

The display of the volume data, employing the TF_{3D}, was realized via GPU-raycasting. For the implementation, principle setups and acceleration strategies, as described in [SHN*06] and [EKE01], were applied. The renderer was implemented with the Luxinia 3D engine (www.luxinia.de), which is scriptable via Lua and uses OpenGL and Cg as rendering backend. Seven seconds are needed from application start to the first visible rendered frame and the achieved frame rate is $\approx$ 50 Hz. High quality shots with eight time finer raysteps are rendered when no interactions are performed and take less than 0.1 seconds. The application was run at 1024×768 on a GeForce 9600 GT 512MB.

5. Informal Evaluation

We applied our techniques to 12 CTA datasets from a 64-slice MSCT scanner (Siemens Sensation 64). The methods and visualizations were discussed with three board-certified radiologists within the scope of an informal evaluation. For comparison, we also provided conventional greyscale images. The datasets were acquired from living persons and gold standards, e.g. histological analyses were not available. For the evaluation, we developed an application using the platform MeVisLab (www.mevislab.de).

To enable the investigation of the datasets, we generated a DVR view with combined 2D views, consisting of a CPR and an MPR view. The CPR and MPR view as well as the 3D visualization of the coronary artery tree are linked with each other. On the one hand, the user can traverse the CPR view with the correspondending MPR view being updated. On the other hand, the user can choose an arbitrary vessel segment in the 3D view with the 2D views being generated accordingly (see Fig. 8).

5.1. Visualization Environment

The evaluation of our prototype included an examination of the DVR views concerning overview visualizations of hard plaques and stents, the investigation of smaller hard plaque deposits (see Fig. 9) and the investigation of stenoses and pathologic changes of the vessel wall in the 3D view (see Fig. 10).

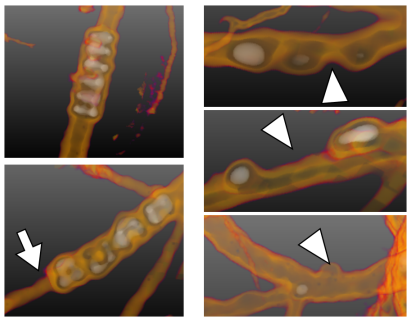

Figure 10: *Stenoses of coronary artery vessels in DVR views. On the left, two coronary stents are depicted. The left bottom picture reveals a stenosis (arrow) at the end of the stent where the left upper picture indicates no stenoses. On the right, pathologic changes of the vessel wall lead to positive and negative remodeling (arrowheads).*

The 2D views were analyzed simultaneously, and we discussed similar topics to the DVR views in more detail, including the overview of hard plaques and stents in CPR views (see Fig. 11), the investigation of a visual separation of smaller hard plaque deposits and pathologic vessel wall changes in CPR views (see Fig. 8 and Fig. 11), and the investigation of MPR views by analyzing the visualization of hard plaques (see MPR views in Fig. 8), stents and noncalcified plaques (see Fig. 12). The presentation of the TF-based visualizations was accompanied with discussions and questions.

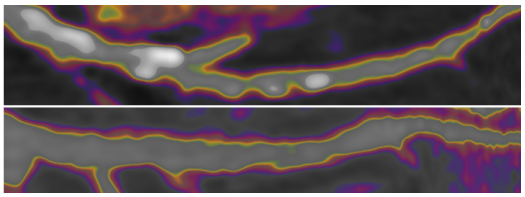

Figure 11: *CPR views of the left anterior descending artery of two datasets. Whereas the first one (top) exhibits a high hard plaque burden, the second one (bottom) does not show hard plaque occurences.*

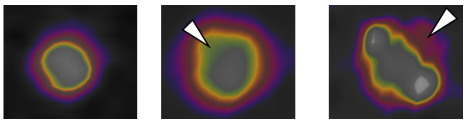

Figure 12: *MPR views provide the cross-sectional views of the coronary arteries. The type of the non-calcified plaque (arrowheads) may be inferred from the color coding: MPR view without plaques (on the left), greenish colors indicate denser structures (middle), whereas pinkish colors indicate lipid accumulations contained in soft plaques (right).*

5.2. Feedback of Clinical Experts

The clinical experts highly appreciate the DVR techniques using the TF_{3D} for the segmented coronary arteries. The fast overview of the complex topology as well as of the patient's overall plaque burden and coronary stents was evaluated as very useful. With the visual separation of even small hard plaques in 2D and 3D views, plaque deposits can be analyzed in more detail. Some smaller hard plaques were not detected with conventional windowing but with a TF_{2D} based view. This is an essential finding since the overall plaque burden is crucial for treatment decisions.

The color coding of the vessel wall was rated high, since the different hues allow a differentiation of densities for the vessel wall with very small volumes. The radiologists prefer the assignment of white and beige colors to dense structures as hard plaques and stents. The opacity mapping of the TF_{3D} and the opacity influenced combination of TF_{2D} and windowing was considered to be beneficial. Whereas the 3D view could direct the user's attention to luminal changes, all radiologists pointed out that evaluation of stenoses requires CPR and MPR views. In 2D views, the possibility to highlight the vessel wall was rated very high, since indications of possible positive or negative remodeling are provided.

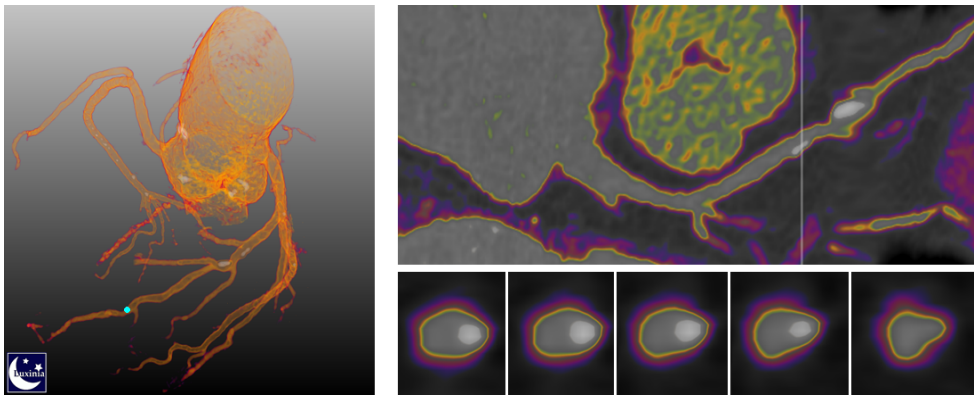

Figure 8: *Layout of the prototype. On the left, the DVR view can be examined by rotating and zooming. The user can pick an arbitrary vessel segment (see cyan sphere) and generate the corresponding CPR and oblique MPR views (right). At the bottom right MPR views orthogonal to the local vessel centerline, starting from the white vertical in the CPR view are shown. The prototype enables the user to switch between conventional windowing visualization and the TF_{3D} and TF_{2D} based visualizations. It is also possible to enlarge single views.*

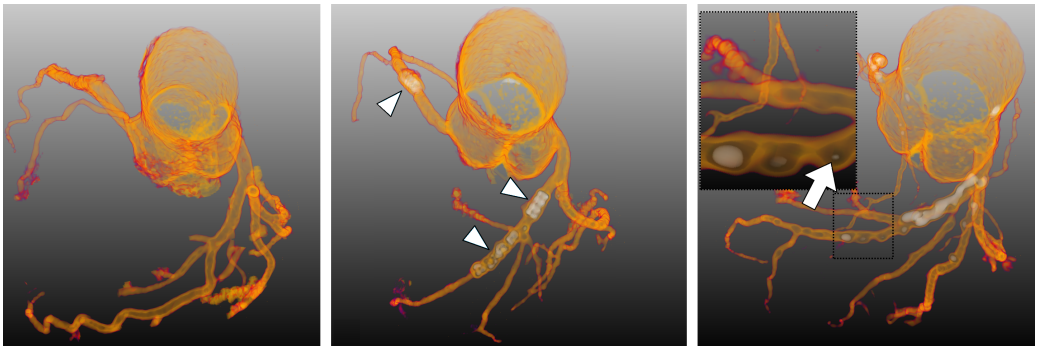

Figure 9: *DVR views of three different datasets. On the left, the DVR view indicates a very low patient's overall plaque burden, since no hard plaques can be seen. The dataset in the middle exhibits three stents (arrowheads), whereas the visualization on the right shows many hard plaques. Even small hard plaques are recognizeable (arrow).*

Two minor drawbacks exist. First, the highlighting of hard plaques in 2D views was critizised by one radiologist. A highlighted hard plaque seems to be surrounded by blood. Since hard plaques contain very dense calcium deposits as well as lipid or fibrous accumulations, they show different intensity values. The intensity values range from values smaller than the contrast-enhanced blood to values larger than the contrast-enhanced blood. Intermediate intensity values will not be highlighted, since they are treated the same way as the blood. Therefore, this problem is inherent to 1D TFs for this scenario. Second, the vessel wall's outer boundary contrast to the surrounding tissue in 2D views was evaluated as too low by one radiologist. We chose low contrast due to the absence of a reliable segmenation.

In conclusion, the radiologists rated the presented techniques as useful extension for evaluation of CTA datasets, since the attention is directed to pathologic changes of the vessel wall and a fast overview is provided. For clinical decision making, a semi-quantitative analysis is necessary, where the presented visualizations are combined with quantitative parameters, e.g. the vessel lumen's diameter.

6. Conclusions & Future Work

We presented a method for the visual emphasis of coronary artery plaque. We developed fully automatically adjusted TFs based on the segmented coronary arteries in CTA image data. The proposed method was also suitable for low quality segmentations, e.g. with data artifacts or poor contrasts. The plaque deposits consist of different accumulations with different densities. Although an automatic segmentation of all plaque types is not possible, we present a method for highlighting hard plaques and soft and fibrous plaques by color

coding of the vessel wall. Also early stages of the CAD consisting of non-stenotic plaque deposits can be visualized.

The adapted TFs were combined with common visualization techniques of CTA datasets. An informal evaluation with three radiologists revealed that our method is a beneficial extension for conventional CTA evaluation. Due to the locally non-uniform spatial diffusion of the contrast medium the presented approach could be the basis for a more sophisticated uncertainty visualization, as presented by [LLPY07]. In addition, size-based TFs as presented by [CM08] could be applied and compared to the presented approach.

Problems arose due to the non-uniform spatial variation of the contrast medium which resulted in different contrast agent accumulations. Potential improvements are the individual creation of a local TF for each vessel segment. In contrast, we expect a loss of quality for smaller branches, since these branches will contain too few voxels for a reliable local histogram analysis via IPV extraction.

Acknowledgements

We thank Dr. Stephan Achenbach (University of Erlangen-Nürnberg, Germany) for providing the image data and MeVis Research for providing advanced MeVisLab features.

References

[AJH*90] AGATSTON A. S., JANOWITZ W. R., HILDNER F., ZUSMER N. R., VIAMONTE M. J., DETRANO R.: Quantification of coronary artery calcium using ultrafast computed tomography. *J Am Coll Cardiol. 15*, 4 (1990), 827–832.

[Ame07] AMERICAN HEART ASSOCIATION: Heart Disease and Stroke Statistics - 2007 Upd. *Circulation 115* (2007), e69–171.

[BA02] BULLITT, AYLWARD S. R.: Volume rendering of segmented image objects. *IEEE Transactions on Medical Imaging 21*, 8 (2002), 998–1002.

[CM08] CORREA C. D., MA K.-L.: Size-based Transfer Functions: A New Volume Exploration Technique. *IEEE Transactions on Vis. and Computer Graphics 14*, 6 (2008), 1380–1387.

[EKE01] ENGEL K., KRAUS M., ERTL T.: High-quality pre-integrated volume rendering using hardware-accelerated pixel shading. In *Proc of the ACM SIGGRAPH/EUROGRAPHICS workshop on Graphics hardware* (2001), ACM, pp. 9–16.

[HBF*05] HENNEMUTH A., BOSKAMP T., FRITZ D., KÜHNEL C., BOCK S., RINCK D., ET AL.: One-click coronary tree segmentation in CT angiographic images. *CARS 2005: Computer Assisted Radiology and Surgery 1281* (2005), 317–321.

[HBS*02] HONG C., BECKER C. R., SCHOEPF U. J., ET AL.: Coronary Artery Calcium: Absolute Quantification in Nonenhanced and Contrastenhanced Multi - Detector Row CT Studies. *Radiology 223* (2002), 474–480.

[KFW*02] KANITSAR A., FLEISCHMANN D., WEGENKITTL R., FELKEL P., GRÖLLER M. E.: CPR - Curved Planar Reformation. In *IEEE Visualization 2002* (2002), pp. 37–44.

[KHB*06] KUEHNEL C., HENNEMUTH A., BOCK S., OELTZE S., BOSKAMP T., KRASS S., ET AL.: New Software Assistants for Cardiovascular Diagnosis. In *GI-Workshop "Softwareassistenten - Computerunterstützung für die medizinische Diagnose und Therapieplanung"* (2006), vol. 1, Springer, pp. 491–498.

[KKH02] KNISS J., KINDLMANN G., HANSEN C.: Multidimensional Transfer Functions for Interactive Volume Rendering. *IEEE Transactions on Visualization and Computer Graphics 8*, 3 (2002), 270–285.

[LLPY07] LUNDSTRÖM C., LJUNG P., PERSSON A., YNNERMAN A.: Uncertainty visualization in medical volume rendering using probabilistic animation. *IEEE Transactions on Vis. and Computer Graphics 13*, 6 (Nov.-Dec. 2007), 1648–1655.

[LLY05] LUNDSTRÖM C., LJUNG P., YNNERMAN A.: Extending and Simplifying Transfer Function Design in Medical Volume Rendering Using Local Histograms. Eurographics Association, pp. 263–270.

[NRJ93] NAPEL S., RUBIN G. D., JEFFREY R. B. J.: STS-MIP: a new reconstruction technique for CT of the chest. *J Comput Assist Tomogr 17*, 5 (1993), 832–838.

[PAM*07] POHLE K., ACHENBACH S., MACNEILL B., ROPERS D., FERENCIK M., ET AL.: Characterization of non-calcified coronary atherosclerotic plaque by multi-detector row CT: Comparison to IVUS. *Atherosclerosis 190* (2007), 174–180.

[PO07] PREIM B., OELTZE S.: *Visualization in Medicine and Life Sciences*. Springer, 2007, ch. 3D Visualization of Vasculature: An Overview, pp. 19–39.

[RSK06] REZK-SALAMA C., KOLB A.: Opacity Peeling for Direct Volume Rendering. *IEEE/Eurographics Symposium on Visualization 25*, 3 (2006), 597–606.

[SB*04] SCHOEPF U. J., BECKER C. R., ET AL.: CT of Coronary Artery Disease. *Radiology 232*, 1 (2004), 18–37.

[SCC*04] STRAKA M., CERVENANSKY M., CRUZ A. L., KOCHL A., SRAMEK M., GROLLER E., FLEISCHMANN D.: The VesselGlyph: Focus & Context Visualization in CT-Angiography. In *IEEE Visualization 2004* (2004), pp. 385–392.

[SHN*06] SCHARSACH H., HADWIGER M., NEUBAUER A., STEFANWOLFSBERGER, BÜHLER K.: Perspective Isosurface and Direct Volume Rendering for Virtual Endoscopy Applications. In *Proc of Eurovis* (2006), pp. 315–322.

[SPSP02] SELLE D., PREIM B., SCHENK A., PEITGEN H.-O.: Analysis of vasculature for liver surgical planning. *Medical Imaging, IEEE Transactions on 21*, 11 (2002), 1344–1357.

[TPD06] TAPPENBECK A., PREIM B., DICKEN V.: Distance-Based Transfer Function Design: Specification Methods and Applications. In *Simulation und Visualisierung* (2006), SCS, pp. 259–274.

[vOvGR*03] VAN OOIJEN P. M. A., VAN GEUNS R. J. M., RENSING B. J. W. M., BONGAERTS A. H. H., ET AL.: Noninvasive Coronary Imaging Using Electron Beam CT: Surface Rendering Versus Volume Rendering. *AJR 180* (2003), 223–226.

[VST*03] VEGA F., SAUBER N., TOMANDL B., NIMSKY C., GREINER G., HASTREITER P.: Enhanced 3D-Visualization of Intracranial Aneurysms Involving the Skull Base. In *Proc. of MICCAI* (2003), vol. 2879 of *LNCS*, Springer, pp. 256–263.

[VST*04] VEGA HIGUERA F., SAUBER N., TOMANDL B., NIMSKY C., ET AL.: Automatic adjustment of bidimensional transfer functions for direct volume visualization of intracranial aneurysms. In *In Proc. of SPIE Conference on Medical Image Computing* (2004), vol. 5367, pp. 275–284.

[WFKF06] WESARG S., FAWAD KHAN M., FIRLE E.: Localizing Calcifications in Cardiac CT Data Sets Using a New Vessel Segmentation Approach. *Journal of Digital Imaging 19*, 3 (2006), 249–257.